JACS
JOURNAL OF THE AMERICAN CHEMICAL SOCIETY
Article
pubs.acs.org/JACS

Electrodeposition of Single Nanometer-Size Pt Nanoparticles at a Tunneling Ultramicroelectrode and Determination of Fast Heterogeneous Kinetics for $Ru(NH_3)_6^{3+}$ Reduction

Jiyeon Kim and Allen J. Bard*

Center for Electrochemistry, Department of Chemistry, The University of Texas at Austin, Austin, Texas 78712, United States

Supporting Information

ABSTRACT: We studied extremely fast kinetics of an outer-sphere heterogeneous electron transfer (ET) reaction at a single Pt nanoparticle (NP) using the newly adapted Kotecký–Levich (K-L) method. In this work, an electrode was prepared by nucleating and growing a single Pt NP on a tunneling ultramicroelectrode (TUME) that produces 1–40 nm or greater dimensions. Such a small-size electrode greatly enhances the mass transfer rate, thus enabling us to reliably determine ET kinetic parameters for fast ET reactions. Based on the recently demonstrated K-L model for a general UME, ET kinetic information could be measured by constructing a plot of 1/current density vs 1/mass transfer rate from the series of steady-state voltammograms obtained using Pt NP-deposited TUMEs. For this K-L plot, we altered the mass transfer rates by varying the electrode size, i.e., the Pt NP size in this work. The determined standard rate constant, k^0, of heterogeneous reduction reaction for $Ru(NH_3)_6^{3+}$ was unprecedentedly high, at 36 ± 4 cm/s, confirmed by theoretical simulation. Extended applications to various electrocatalytic reactions with different types of electrodeposited metal NPs will show the versatility of our approach. Particularly, this novel fabrication of a nanometer-sized electrode and its application to fast ET kinetic study with simple instrumentation should be useful in studies of particle size and structure effects on given catalytic reactions.

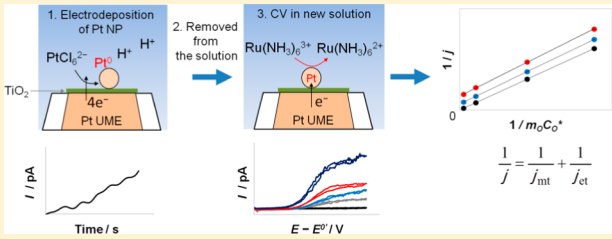

INTRODUCTION

Reported heterogeneous electron transfer (ET) rate constants in electrochemistry are remarkably irreproducible. While some of this might be caused by the heterogeneity and contamination problems of electrode surfaces, it is also true for outer-sphere reactions that are less sensitive to electrode surface effects. A significant problem is that the measured rate of electrode reactions depends upon both the rate of mass transfer and the inherent ET rate constant, so that measurements of large rate constants require complete elimination of contributions from mass transfer (as well as other factors, e.g., uncompensated resistance). Indeed, published ET rate constants for a given fast reaction have tended to increase over the years as electrochemical methodology has improved, and a number of reports have described approaches to measuring rapid electrochemical ET reactions. By far, the Mirkin group reported the fastest standard rate constant, k^0 = 17 cm/s, for $Ru(NH_3)_6^{3+}$ using nanoelectrodes as a probe for scanning electrochemical microscopy (SECM).[1] Recently, the Amemiya group also measured k^0 up to 17 cm/s for $FcTMA^+$ with highly oriented pyrolytic graphite (HOPG) by employing nanogap voltammetry with SECM at a stabilized nanogap.[2] In those works, mass transfer rates could be highly enhanced by creating tens of nanometer-size gaps as well as nanoelectrodes; thereby fast ET kinetics could be reliably studied. Certainly, utilization of nm-size electrodes or gaps enhances mass transfer rates without the need for convection.[1,3] For example, nm-size electrodes or nanogaps can offer mass transfer rate constants of tens of cm/s, allowing the measurement of k^0 in a comparable range. However, the preparation of nm-size electrodes with known well-defined geometry, or maintaining nm gaps, is not trivial. Here, we propose electrodepositing a Pt nanoparticle (NP) on a tunneling ultramicroelectrode (TUME) to easily achieve nm dimensions, where an active site is limited to the surface of the Pt NP. This approach allows for fabrication of electrodes with radii of a few to tens of nm.

Subsequently, we apply a Pt NP-deposited TUME (Pt NP/TUME) to the kinetic study of heterogeneous ET reaction of $Ru(NH_3)_6^{3+}$ as a model redox mediator using steady-state voltammetry. In this kinetic study, we employ our newly demonstrated Kotecký–Levich (K-L) method,[4] where a series of steady-state voltammograms from various sized Pt NP/TUMEs are used to construct a plot of 1/current density (j) vs 1/mass transfer rate (m) at different potentials to extract the kinetic information. (In this work, we used a different formulism using a formal potential, $E^{0\prime}$, instead of an equilibrium potential, E_{eq}.) In addition to the absolute value of the rate constant, researchers are also interested in particle size effects on the relative rate constants and also on mass transfer. The methods described here can also be useful in this application.

Received: November 11, 2015
Published: January 5, 2016

DOI: 10.1021/jacs.5b11655
J. Am. Chem. Soc. 2016, 138, 975–979

EXPERIMENTAL SECTION

Chemicals and Materials. Ruthenium hexaammonium chloride ($Ru(NH_3)_6Cl_3$), hexachloroplatinic acid (H_2PtCl_6), and $TiCl_3$ (reagent grade) were purchased from Sigma-Aldrich and used as received. Ferrocenemethanol (FcMeOH, Sigma-Aldrich) was recrystallized in hexane before using it. Potassium nitrate (KNO_3) and sulfuric acid (H_2SO_4) were obtained from Fisher Scientific. A Milli-Q Integral system (EDM Millipore, Billerica, MA) was equipped to obtain ultrapure water with total organic carbon (TOC) level at less than 3 ppb, as measured by an internally equipped TOC monitor as well as the resistivity of 18.3 MΩ/cm. All the solutions for electrochemical measurement were prepared with ultrapure water and filtrated with a syringe filter with 100 nm diameter pore (Millipore).

TUME Fabrication. A Pt UME was fabricated by using a CO_2-laser puller, a microforge, and a focused ion beam (FIB) instrument as reported elsewhere.[5] Further, a TiO_2 layer was electrochemically deposited on Pt UME as reported elsewhere.[7] Briefly, the TiO_2 layer was anodically electrodeposited at a constant potential of 100 mV + open circuit potential (OCP) in 5 mM $TiCl_3$ solution at pH 2.3 under deaerated condition with Ar purging. After each 3 s deposition, the electrochemical response of Pt UME was monitored in 1 mM FcMeOH, 0.1 M KNO_3 to check the passivation of conductive Pt surface. After ca. 97% of passivation, Pt UME was dried overnight in air at room temperature to further dehydrate and convert Ti(VI) oxopolymer to TiO_2. The resulting electrode (TUME) after overnight drying shows full passivation, i.e., no faradaic current response in 5 mM $Ru(NH_3)_6^{3+}$, 0.1 M KNO_3 under desecrated condition. To avoid any damage of electrode caused by electrostatic discharge and electrochemical etching, we handled TUME with protection tools as well as "cell on between runs" function as reported elsewhere.[6] Also, the relative humidity was maintained over 30% at 22−24 °C.

Electrochemical Measurements. A CHI920c bipotentiostat (CH Instruments, Austin, TX) was used for electrochemistry. To deposit a Pt NP on the TUME, the TUME was immersed in 100 μM H_2PtCl_6, 5 mM H_2SO_4 solution or 10 μM H_2PtCl_6, 0.5 mM H_2SO_4 solution with applied potential at 0.75 V vs Ag/AgCl. Using multiple potential step techniques, a constant potential of 0.15 or −0.27 V vs Ag/AgCl was applied during electrodeposition respectively under a two-electrode system. After a certain induction time, when the transient current was rising, the technique is manually stopped to quit the growth of Pt NP, where the potential returned to the original potential value, 0.75 V. For this potential control, "return to the initial potential after run" function was used. Once Pt NP/TUME was prepared, the steady-state voltammograms were obtained in 5 mM $Ru(NH_3)_6^{3+}$, 0.1 M KNO_3 under desecrated condition. To avoid any electrode damage, we handled TUME with protection tools as well as the "cell on between runs" function as reported elsewhere.[7] Also, the relative humidity was maintained over 30% at 22−24 °C.

RESULTS AND DISCUSSION

Nucleation and Growth of Pt NP on Tunneling TiO_2 Film. The overall schematics of an electrode fabrication are presented in Figure 1. Using a TUME with a ca. 1 nm thick TiO_2 layer prepared as reported previously,[7] we electrodeposited a single Pt NP in acidic Pt precursor solution by applying a constant potential. After a certain induction time, the formation and the growth of a stable single Pt particle can be monitored by recording current−time transients during a deposition process as shown in Figure 2. This electrodeposition was performed in 100 μM H_2PtCl_6, 5 mM H_2SO_4 solution or 10 μM H_2PtCl_6, 0.5 mM H_2SO_4 solution at a constant potential of 0.15 or −0.27 V vs Ag/AgCl, respectively. At a small cathodic potential with 100 μM H_2PtCl_6, the transient current response shows kinetically controlled behavior with quadratic dependence on time (t), while a mass transfer controlled behavior with $t^{1/2}$ dependence was observed at a large cathodic potential in 10 μM H_2PtCl_6.[8−10] These transient currents were quantitatively analyzed by

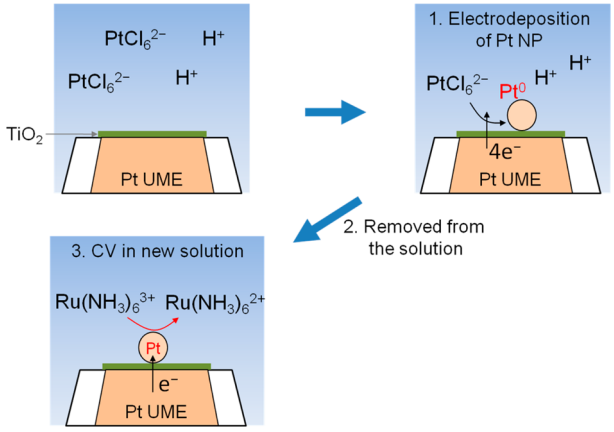

Figure 1. Schematics of the fabrication and the characterization of Pt NP/TUME by electrodepositing a single Pt NP on TUME, removal of Pt NP/TUME from the solution, and running cyclic voltammetry in new solution of $Ru(NH_3)_6^{3+}$.

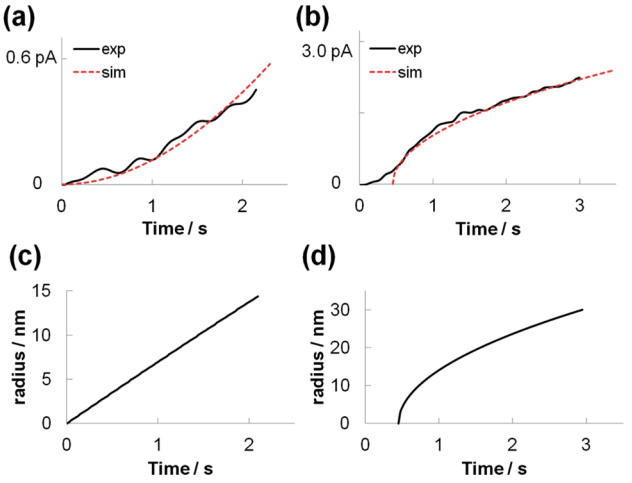

Figure 2. Current−time transients for the electrodeposition of a single Pt NP on TUME from a solution of (a) 100 μM H_2PtCl_6, 2 mM KNO_3, and 5 mM H_2SO_4 at 0.15 V vs Ag/AgCl, and (b) 10 μM H_2PtCl_6, 2 mM KNO_3, and 0.5 mM H_2SO_4 at −0.27 V vs Ag/AgCl. Each experimental curve well agreed with theoretical curves using eq S1. (c,d) Theoretically predicted radii as a function of time at each corresponding E_{eff} using eq S2.

adapting Kucernak and co-workers' model, where a transient current during nucleation and growth of a single Pt cluster on carbon could be explained as a function of the precursor concentration, time, and potential (see eq S1 in the Supporting Information (SI)).[8] Both experimental current responses agreed well with theoretically simulated values at a given time and concentration (red dotted curves in Figure 2a,b; more details are in the SI). In this analysis, we could determine the effective potential (E_{eff}) as 0.091 and 0.51 V for Figure 2a,b, respectively, exerted on TUME during nucleation and growth of a Pt cluster (see SI). These E_{eff} are needed to theoretically predict a Pt NP radius as a function of time using Kucernak's approach (see eq S2 in the SI). In Figure 2c,d, a change in a Pt NP radius as a function of t at E_{eff} = 0.091 and 0.51 V is plotted, where the radii at the end time point are 14.4 and 30.0 nm, respectively. In parallel, the radius of a Pt NP also can be estimated from the integrated charges, Q in experimental current transients assuming a spherical geometry and 100% deposition efficiency:

DOI: 10.1021/jacs.5b11655
J. Am. Chem. Soc. 2016, 138, 975−979

$$r = \sqrt[3]{\frac{3QV_a}{4\pi nq}} \quad (1)$$

where r is the radius of a Pt NP, V_a is the atomic volume of Pt (2.32×10^{-29} m^3), q is the elementary charge, and n is the number of transferred electrons ($n = 4$). The resulting radii from Figure 2a,b were 14.0 and 28.7 nm, respectively, consistent with the theoretical estimation above suggesting the validity of determined E_{eff} in a given system.

These Pt NPs were visually confirmed by scanning electron microscopy (SEM) and with a focused ion beam (FIB). Single Pt NPs of ca. 13 and 28.5 nm radii on each TUME were seen with nearly spherical geometry (Figure 3). Notably, the observed

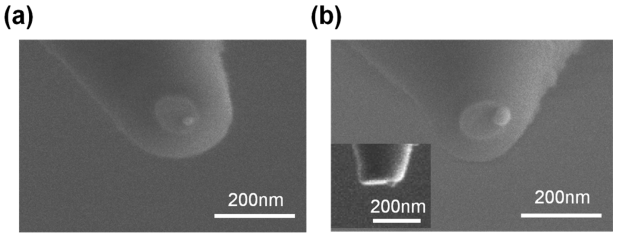

Figure 3. SEM images of (a) ~13 nm and (b) 28.5 nm radius Pt NPs on TUMEs. The inset in panel b shows a focused ion beam image, with the side view of a Pt NP on TUME.

dimensions are close to the estimated radii from both the integrated charges and theoretical calculation based on Kucernak's approach, indicating that most of transient currents could be attributed to the formation and growth of a Pt NP. It also verifies theoretically determined E_{eff}.

Voltammetric Characterization. In addition, we electrochemically characterized Pt NP/TUME by steady-state voltammetry in 5 mM $Ru(NH_3)_6^{3+}$, 0.1 M KNO_3. Including above Pt NPs/TUME, a series of Pt NP/TUMEs were studied, which were prepared as above. The radius of Pt NP on TUME was estimated from a limiting current in obtained voltammograms assuming a single Pt NP with a spherical geometry on a planar surface,[3,11]

$$i_{lim} = 4\pi(\ln 2)nFDC^* r \quad (2)$$

where i_{lim} is a limiting current, F is the Faraday constant (96 485 C/mol), D is the diffusion coefficient of $Ru(NH_3)_6^{3+}$ (7.4×10^{-6} cm^2/s), C^* is the bulk concentration (5 mM) with the number of electrons transferred, $n = 1$, in the ET reaction, and r is the radius of a single Pt NP. The resulting radii of Pt NP range from 0.7 to 41.6 nm. The 0.7−1.6 nm radius Pt NPs were prepared at a small potential, $E_{eff} = 0.091$ V (or $E = 0.15$ V vs Ag/AgCl), while a large potential, $E_{eff} = 0.51$ V (or $E = -0.27$ V vs Ag/AgCl), was used for the >3 nm radius NP. Their voltammograms are presented in Figure 4, where $E^{0'} = -0.197$ V vs Ag/AgCl. $E^{0'}$ was independently determined by cyclic voltammetry (CV) at 20 mV/s with a 25 μm diameter Pt UME (data not shown). In Figure 4a, a current response from a bare TUME with a pinhole free TiO_2 blocking layer is shown to ensure that all faradaic currents are attributed to Pt NPs not a leakage on TUME (also see Figure S1 in the SI).

To rationalize our assumption of a single Pt NP in its radius estimation, we introduce a nucleation exclusion zone representing an area where the nucleation rate has dropped by 1 order of magnitude surrounding a growing particle as reported elsewhere.[8] Using Kucernak's theoretical model, we plotted a

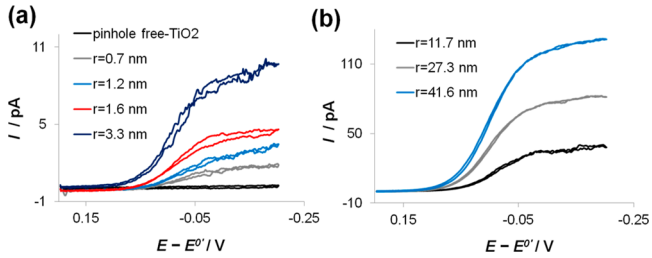

Figure 4. Cyclic voltammograms of (a) bare TUME with a pinhole free TiO_2 layer and radii of 0.7−3.3 nm Pt NP/TUME and (b) radii of 11.7−41.6 nm Pt NP/TUME in 5 mM $Ru(NH_3)_6^{3+}$, 0.1 M KNO_3.

dimensionless size of nucleation exclusion zone (ρ) with respect to the actual size of the particle (r) as a function of t at given potentials and precursor concentrations (Figure 5a, also see SI).

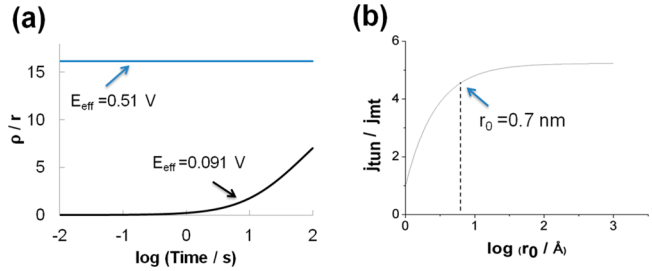

Figure 5. (a) Plot of dimensionless nucleation exclusion zone (ρ) with respect to the radius of a particle (r) as a function of time at each potential, E_{eff} = 0.51 and 0.091 V. (b) Ratio of tunneling and electrochemical (mass transfer-controlled) current densities as a function of a particle radius, r_0, at a given TiO_2 thickness, w_0 = 10.5 Å (see SI). Dotted line denotes 0.7 nm radius of Pt NP.

When a particle is growing under diffusion control at $E_{eff} = 0.51$ V with 10 μM $PtCl_6^{2-}$ (Figure 2b), the nucleation probability is almost instantaneously reduced by 1 order of magnitude within ca. 16 times the radius of the growing particle (blue curve in Figure 5a). This means that it is unlikely to have another nucleation within 80 nm distance around a 5 nm radius particle. Such a nucleation exclusion zone helps the production of a single nucleus, since there will be a significant reduction in the precursor concentration surrounding a growing particle, thus reduce the probability of nucleating another new particle. In that sense, a small electrode, large potential, and low precursor concentration are crucial criteria to form a single particle. The experimental conditions used for larger than 3 nm radius Pt NP meet these criteria, hence the utilization of a small TUME with ca. 100 nm diameter, potential as large as $E_{eff} = 0.51$ V, and low precursor concentration of 10 μM levels could maximize the possibility to form a single NP. That explains why we could see only one NP on a TUME in SEM images (Figure 3).

In contrast, when the growth of particle is under kinetic control at $E_{eff} = 0.091$ V and 100 μM $PtCl_6^{2-}$ (Figure 2a), the nucleation exclusion zone only reaches within a few radii of a growing particle even after appreciable time (black solid curve in Figure 5a), which means that it could be possible to form multiple smaller nuclei at other points in a given area on the TUME. In fact, this latter condition was used to form 0.7 to 1.6 nm radius Pt NPs on a TUME. In this case, two factors, instability of Pt nuclei and tunneling effect, should be considered to verify the assumption of a single particle. The 1.4 nm diameter Pt NP, the smallest obtained here, nearly exceeds the critical size of ca. 1

DOI: 10.1021/jacs.5b11655
J. Am. Chem. Soc. 2016, 138, 975−979

nm diameter for a stable Pt nucleus, corresponding to 30−40 atoms.[12] Accordingly, any smaller nuclei than 1 nm diameter could dissolve into the solution due to instability (Ostwald ripening).[8,13] Moreover, in a TUME system, the tunneling can affect an overall current response depending on a Pt NP size. At radii of Pt NPs larger than 0.7 nm, the overall current response on a TUME with ca. 1 nm thick TiO_2 layer is mainly governed by electrochemical control as studied in the previous work[7,14] (Figure 5b, also see SI). As the Pt NP radius becomes smaller than 0.7 nm, tunneling becomes a more significant factor in the overall current, thus causing a smaller mass transfer limited current. Since the mass transfer limited current at a 0.7 nm radius Pt NP in 5 mM $Ru(NH_3)_6^{3+}$ is 1.8 pA, almost reaching the detection limit of our present potentiostat, no appreciably detectable current is expected from smaller nuclei with significant tunneling influence. Thereby, considering these factors of instability and tunneling effect, a contribution of multiple nuclei smaller than 0.7 nm radii should be negligible to the overall current response. Other factors may also come into play in considering the number of particles formed. These include the number of nucleation sites on the surface and the rate of 2D diffusion of metal atoms on the electrode surface. Overall, it seems reasonable that we assume solely a single Pt NP formed under any experimental condition here corresponding to the limiting current in obtained voltammograms.[8−10,15]

Determination of the Rate Constant for $Ru(NH_3)_6^{3+/2+}$ Reaction. Once each radius of single Pt NPs was determined, we further analyzed obtained steady-state voltammograms to extract the kinetic information using newly adapted K-L method for general UMEs. In this K-L treatment, we considered the overall current density at a Pt NP/TUME governed by the rates of three consecutive processes of (a) a direct tunneling from Pt UME to Pt NP through the TiO_2 layer, (b) a mass transfer of redox species from bulk solution to near a Pt NP surface, and (c) an ET to redox species at Pt NP. Since the tunneling rate at any given size of a Pt NP here across ca. 1 nm thick TiO_2 layer is very high, the resulting current density at Pt NP is mainly controlled by mass transfer (MT) and ET as previously reported[14] (see SI). Consequently, the overall current density at Pt NP can be expressed as

$$\frac{1}{j} = \frac{1}{j_{ET}} + \frac{1}{j_{MT}} \tag{3}$$

For a quasi-reversible one-step, one-electron reduction reaction,

$$O + e^- \underset{k_b}{\overset{k_f}{\rightleftarrows}} R \tag{4}$$

The overall current density can be written as reported previously,[4]

$$\frac{1}{j} = \frac{1}{Fk^0C^*}\frac{b^\alpha}{1-pb} + \frac{1}{FmC^*}\frac{1+qb}{1-pb} \tag{5}$$

where $b = e^{(F/RT)(E-E^{0'})}$, $C^* = C_O^*$, $C_R^* = pC_O^*$, $m = m_O$, and $m_O/m_R = q$. Notably, eq 5 is analogous to eq 3 of K-L treatment. In our approach, the size of the UME, i.e., the size of Pt NP in this work, is varied to alter the mass transfer rate, m. Hence, we can construct a plot of $1/j$ vs $1/mC^*$, as called K-L plot at given different potentials. The averaged currents from forward and reverse curves in Figure 4a were chosen due to a significant noise level, which caused a maximum ca. 4% deviation among the highest and lowest currents at given potential. A set of linear K-L plots are obtained with a constant slope of $\sim 1/F$ and different y-intercepts as presented in Figure 7a (below), where potential ranges of $E-E^{0'} \leq -0.05$ V are used[4] in CVs from 0.7 to 3.3 nm radius Pt NP/TUMEs. In this potential range, b becomes negligibly small close to 0, thus a resulting slope of K-L plots should be $1/F$. At large potential as −0.2 V, mass transfer dominates, so that a linear K-L plot intersects the origin. As the potential becomes smaller, the y-intercept, $\frac{1}{Fk^0C^*}\frac{b^\alpha}{1-pb}$, deviates more from the origin due to a greater contribution of kinetic control. Noticeably, the y-intercepts in $Ru(NH_3)_6^{3+}$ reduction reaction are small implying a rapid heterogeneous ET reaction. From a set of y-intercepts in the potential range from −0.15 to −0.05 V, we could estimate k^0 unprecedentedly high as 36 ± 4 cm/s with α = 0.47, where p = 0.01 to 0.001 and q = 1 are assumed. Notably, the assumption of p ranging from 0.01 to 0.001 as a realistic concentration level based on a nearly zero initial current in CVs does not affect the obtained rate constant due to a negligibly small b in the given potential range. In this estimation, α value was numerically determined from the potential dependence of the y-intercepts independent of the k^0 value. With the y-intercept given above and $pb \ll 1$, we can derive the equation,

$$\ln(y\text{-intercept}) = \ln\left(\frac{1}{Fk^0C^*}\right) + \frac{\alpha F}{RT}(E - E^{0'}) \tag{6}$$

By plotting $\ln(y\text{-intercept})$ vs $(E - E^{0'})$, both α and k^0 could be independently determined from the obtained slope and new y-intercept, respectively (Figure 6).

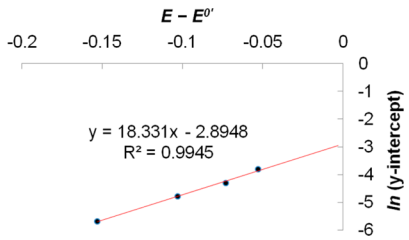

Figure 6. Linear plot of $\ln(y\text{-intercept})$ vs $(E - E^{0'})$ obtained from K-L analysis. Both α and k^0 could be independently determined from the obtained slope and new y-intercept, respectively.

We confirmed these measured kinetic parameters with finite element analysis using COMSOL MULTIPHYSICS (v. 4.2a). As presented in Figure 7b, the simulated voltammograms for k^0 = 36 cm/s, α = 0.5 showed good agreement with experimental curves from the smallest, 0.7 nm to the largest radius, 41.6 nm of Pt NP/TUME. A clear transition from almost nernstian behavior to kinetic control can be seen in the normalized voltammograms with respect to each limiting current. All spans of CVs with various radii of Pt NP/TUMEs also showed good agreement with simulated values with given kinetic parameters, therefore the exceptionally high k^0determined here for the ET reaction of $Ru(NH_3)_6^{3+}$ could be verified (also see Figure S3 in the SI).

Note that within the particle range shown in Figure 7, we found no dependence of k^0 on particle radius. We could create present K-L plots as a multidimensional plot in one graph including current densities, mass transfer rates, different potentials, and different sizes of NPs or electrodes, which would be particularly useful to study the size effect of NP catalysts or nanoelectrodes in a given heterogeneous ET

DOI: 10.1021/jacs.5b11655
J. Am. Chem. Soc. 2016, 138, 975−979

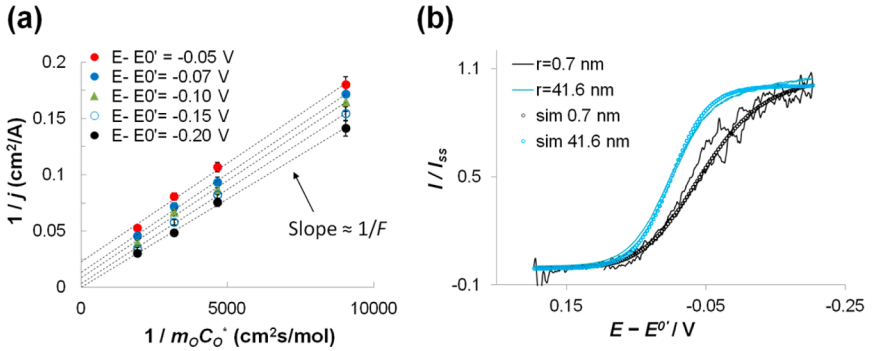

Figure 7. (a) K-L plots generated from CVs in Figure 4a. (b) Theoretically simulated voltammograms for k^0 = 36 cm/s, α = 0.5 fitted with experimental curves from radii of 0.7 and 41.6 nm Pt NP/TUMEs. To show the clear difference in curve shape, voltammograms were normalized respect to each limiting current.

reaction. It is because the constraint of the slope, $1/F$ in K-L plot can be used to evaluate whether the present ET system deviates from linearity, especially as the NP or nanoelectrode becomes smaller.

CONCLUSION

In summary, we report the novel fabrication of a nanometer-sized electrode and its application to an extremely fast kinetic study with a simple ET step, an outer-sphere redox mediator using simple instrumentation. The extension of this approach to an inner-sphere redox reaction undergoing surface-sensitive electrocatalytic reactions will be more complicated but might be able to reveal the heterogeneous and dynamic behavior of NP as a catalyst.[16] Moreover, we hope to apply general electrodeposition methods of other metal NPs to TUME systems.[17−19] This will involve electrodepositing various types of metal NPs with varying sizes on the TUMEs and will demonstrate the versatility of this approach to study diverse catalytic reactions at a distinct NP catalyst. In that sense, this approach should be particularly useful in studying particle composition, size, and structure effects in a given catalyst.[20−22]

ASSOCIATED CONTENT

Supporting Information

The Supporting Information is available free of charge on the ACS Publications website at DOI: 10.1021/jacs.5b11655.

Quantitative analysis of current−time transients for the electrodeposition of a single Pt NP on TUME; nucleation exclusion zone and a single Pt NP; intactness of TUME studied by voltammetry; electrochemistry vs tunneling at a given Pt NP; and simulated voltammograms fitted with experimental curves at given Pt NP/TUME (including eqs S1−S7 and Figures S1−S3) (PDF)

AUTHOR INFORMATION

Corresponding Author

*ajbard@cm.utexas.edu

Notes

The authors declare no competing financial interest.

ACKNOWLEDGMENTS

We acknowledge support of this research from the AFOSR MURI (FA9550-14-1-0003) and the Robert A. Welch Foundation (F-0021). We also thank N. Nioradze and C. M. Hill for helpful discussion. We acknowledge Damon Smith for use of a dual-beam FIB instrument in the Department of Chemical Engineering, Texas Materials Institute, Center for Nano & Molecular Science and Technology, The University of Texas at Austin, and NSF, the Petroleum Research Fund, and Welch Foundation for support of the facilities utilized in this work.

REFERENCES

(1) Sun, P.; Mirkin, M. V. *Anal. Chem.* **2006**, *78*, 6526−6534.
(2) Nioradze, N.; Chen, R.; Kurapati, N.; Khvataeva-Domanov, A.; Mabic, S.; Amemiya, S. *Anal. Chem.* **2015**, *87*, 4836−4843.
(3) Bard, A. J.; Faulkner, L. R. *Electrochemical Methods: Fundamentals and Applications*, 2nd ed.; John Wiley & Sons: New York, 2001.
(4) Kim, J.; Bard, A. J. *Anal. Chem.* **2015**, DOI: 10.1021/acs.analchem.5b03965.
(5) Kim, J.; Izadyar, A.; Nioradze, N.; Amemiya, S. *J. Am. Chem. Soc.* **2013**, *135*, 2321−2329.
(6) Nioradze, N.; Chen, R.; Kim, J.; Shen, M.; Santhosh, P.; Amemiya, S. *Anal. Chem.* **2013**, *85*, 6198−6202.
(7) Kim, J.; Kim, B.-K.; Cho, S. K.; Bard, A. J. *J. Am. Chem. Soc.* **2014**, *136*, 8173−8176.
(8) Chen, S.; Kucernak, A. *J. Phys. Chem. B* **2003**, *107*, 8392−8402.
(9) Li, L. J.; Fleischmann, M.; Peter, L. M. *Electrochim. Acta* **1989**, *34*, 459.
(10) Hills, G. J.; Schiffrin, D. J.; Thompson, J. *Electrochim. Acta* **1974**, *19*, 657.
(11) Bobbert, P. A.; Wind, M.; Vlieger, J. *Phys. A* **1987**, *141*, 58−72.
(12) Gloaguen, F.; Leger, J. M.; Lamy, C.; Marmann, A.; Stimming, U.; Vogel, R. *Electrochim. Acta* **1999**, *44*, 1805.
(13) Zoski, C. G. *Handbook of electrochemistry*, 1st ed.; Elsevier: Amsterdam, 2007.
(14) Hill, C. M.; Kim, J.; Bard, A. J. *J. Am. Chem. Soc.* **2015**, *137*, 11321−11326.
(15) Fleischmann, L.; Li, L. J.; Peter, L. M. *Electrochim. Acta* **1989**, *34*, 475.
(16) Bard, A. J. *J. Am. Chem. Soc.* **2010**, *132*, 7559−7567.
(17) Walter, E. C.; Murray, B. J.; Favier, F.; Kaltenpoth, G.; Grunze, M.; Penner, R. M. *J. Phys. Chem. B* **2002**, *106*, 11407−11411.
(18) Walter, E. C.; Zach, M. P.; Favier, F.; Murray, B. J.; Inazu, K.; Hemminger, J. C.; Penner, R. M. *ChemPhysChem* **2003**, *4*, 131−138.
(19) Galhenage, R. P.; Yan, H.; Tenney, S. A.; Park, N.; Henkelman, G.; Albrecht, P.; Mullins, D. R.; Chen, D. A. *J. Phys. Chem. C* **2013**, *117*, 7191−7201.
(20) Hvolbaek, B.; Janssens, T. V. W.; Clausen, B. S.; Falsig, H.; Christensen, C. H.; NØrskov, J. K. *Nano Today* **2007**, *2*, 14−18.
(21) Zhou, X.; Xu, W.; Liu, G.; Panda, D.; Chen, P. *J. Am. Chem. Soc.* **2010**, *132*, 138−146.
(22) Isaifan, R. J.; Ntais, S.; Baranova, E. A. *Appl. Catal., A* **2013**, *464−465*, 87−94.

DOI: 10.1021/jacs.5b11655
J. Am. Chem. Soc. 2016, 138, 975−979